Limnol. Oceanogr., 52(2), 2007, 739–752

Investigation of the optical backscattering to scattering ratio of marine particles in relation to their biogeochemical composition in the eastern English Channel and southern North Sea

Hubert Loisel[1] *and Xavier Mériaux*
Laboratoire Ecosystème Littoraux et Côtiers, FRE ELICO 2816, 62930 Wimereux, France

Jean-François Berthon
European Commission–DG Joint Research Centre, Institute for Environment and Sustainability, Global Environment Monitoring Unit, 21020 Ispra, Italy

Antoine Poteau
Laboratoire Ecosystème Littoraux et Côtiers, FRE ELICO 2816, 62930 Wimereux, France

Abstract

The variability of the backscattering to scattering ratio of marine particles, $b_{bp}:b_p$, is examined from in situ measurements performed during the spring and early summer of 2004 in the eastern English Channel and southern North Sea. This area is characterized by a quasi-permanent background of mineral matter from direct inputs, or resuspension effects, and by relatively intense spring phytoplankton blooms (mainly diatoms and the prymnesiophyte *Phaeocystis globosa*). The $b_{bp}:b_p$ surface values range between 0.0024 and 0.0417, with a mean value of 0.0138 ± 0.0083. In order to interpret such a great variability, simultaneous water samples were collected for the biogeochemical characterization of the bulk suspended particle population. We show that the $b_{bp}:b_p$ variability is related to the composition of the particulate assemblage expressed by Chl *a*, the POC : SPM and POC : Chl *a* ratios, where Chl *a*, POC, and SPM are the concentrations of chlorophyll *a*, particulate organic carbon, and suspended particulate matter, respectively. Low $b_{bp}:b_p$ values are observed for a particle population dominated by low refractive index material such as phytoplankton, whereas high $b_{bp}:b_p$ values are generally observed in presence of relatively high concentration of inorganic particles. The amount of organic material (both living and nonliving, including phytoplankton) relative to phytoplankton has a strong (and sometimes the greatest) effect on the backscattering-to-scattering ratio. Assuming that phytoplankton and detritus have similar refractive index, this pattern is interpreted as resulting from changes in the particle size distribution as well as by aggregation of mineral and nonliving organic detrital material.

The backscattering coefficient (b_b; m^{-1}) and the detailed understanding of its variability in natural waters are of fundamental importance for oceanographic sciences related to the knowledge of suspended marine particles. The backscattering coefficient is also of primary importance for remote sensing of ocean color, as the radiometric signal recorded by a sensor onboard an aircraft or a satellite is directly proportional to its intensity. However, "our present-day interpretation and detailed understanding of major sources of backscattering and its variability in the ocean are uncertain and controversial" (Stramski et al. 2004). Until the recent development of commercial in situ instrumentation, our knowledge on the light backscattering properties of marine particles relied mostly on theoretical studies based on Mie scattering theory, occasionally combined with laboratory measurements (Stramski et al. 2004 and references therein). Based on these different studies, one may stress that the bulk backscattering coefficient is, to first order, proportional to the particles load and, to second order, to the size distribution, refractive index (determined by the chemical composition), structure, and mean shape of the particle assemblage. Outside bloom conditions—and considering marine particles as homogeneous spheres—nonliving submicron particles are believed to be the dominant source of the particulate backscattering coefficient (b_{bp}; m^{-1}) in the open ocean surface waters (Morel and Ahn 1991; Stramski and Kieffer 1991). This is because these small particles are present at a much higher concentrations than any other particle type. It is usually admitted that this pool of small particles is composed mainly of nonliving particles originating from the decomposition of dead phytoplankton cells and zooplankton detritus. However, because of their high refractive index, submicron mineral particles may be the main contributor to b_{bp}, especially in coastal areas. For an extensive review of the different sources of backscattering in the ocean, one may refer to Stramski et al. (2004), where an evaluation of the role

[1] Corresponding author (hubert.loisel@univ-littoral.fr).

Acknowledgments

We are grateful to the crews of Côte de la Manche. We thank Cédric Boulart, Benoît Gaurier, and Laurent Boudesseul for their help during measurements. Marcel Babin and Grigor Obolensky are also thanked for their ac-9 data collected in 2003. Giuseppe Zibordi and Dirk van der Linde from JRC are acknowledged for their collaboration during the June 2004 campaign. We are particularly grateful to Mike Twardowski for his very pertinent comments on the manuscript. We also thank an anonymous reviewer for valuable comments on the manuscript. This research was funded by the two following French scientific programs: PNEC and ACI-observation de la Terre.

of the various seawater constituents in this process is provided. Note that the relatively small contribution of living phytoplankton to b_{bp} is still controversial, as both Mie calculations performed with layered spheres (Kitchen and Zaneveld 1992; Zaneveld and Kitchen 1995) instead of homogeneous spheres (Morel and Ahn 1991; Stramski and Kieffer 1991), as well as recent laboratory measurements (Vaillancourt et al. 2004), showed that phytoplankton may be more efficient backscatterers than usually assumed. Under bloom conditions, the contribution of phytoplankton cells to the backscattering process is greatly enhanced and may even be the major one for very intense algal blooms (McLeroy-Etheridge and Roesler 1998).

In contrast to the backscattering coefficient, the scattering coefficient (b; m^{-1}) has been the object of numerous studies performed in both oceanic and coastal waters (see references in Loisel and Morel 1998; Babin et al. 2003). Mie calculations showed that the scattering coefficient by particles (b_p) is dominated largely (by more than 95%) by particles of diameter comprised between 0.5 and 10 μm in diameter, assuming a marine particle population presenting a mean index of refraction of 1.05 and a Junge type size distribution with an exponent close to -4 (Stramski and Kieffer 1991). The dependence of b_p on the chlorophyll a concentration (Chl a; mg m^{-3}), usually used to specify the bio-optical state of a water body, has been extensively investigated for open ocean waters (Loisel and Morel 1998 and references therein). Such studies were motivated mostly by the analysis of biogeochemical processes occurring in the water column and by the interpretation of ocean color measurements through the development of semianalytical algorithms. Similar studies were also performed to investigate the relationships between $b_p(\lambda)$ and the particulate organic carbon, POC (Gardner et al. 1993; Loisel and Morel 1998; Claustre et al. 1999). Most of these studies were conducted in open oceanic waters through the classical measurement of the particle attenuation coefficient at 660 nm, $c_p(660)$ (m^{-1}), which may be considered as an excellent proxy for b_p at this peculiar wavelength (Loisel and Morel 1998). Because of the rapid development of in situ instrumentation, some recent fieldwork was also performed in order to explore the b_p spectral dependence and the light-scattering properties of marine particles in relation to the particle mass concentration (Barnard et al. 1998; Gould et al. 1999; Babin et al. 2003).

Other studies have demonstrated that the combination of b_p and b_{bp} (or some equivalent quantities, such as the scattering coefficient at 45° and the total concentration of particles) may be used to characterize the bulk refractive index of the particulate pool, n (Brown and Gordon 1973). Based on such observations, measurements of the particulate backscattering ratio, $b_{bp}:b_p$, have recently been used to describe the variability of n in various oceanic environments (Twardowski et al. 2001; Boss et al. 2004; Sulivan et al. 2005). Note that the backscattering ratio also depends on the relative proportion between small size and large size particles (Ulloa et al. 1994). The higher the proportion of small size particles is, the higher $b_{bp}:b_p$ value is expected. For this reason, Twardowski et al. (2001) established an analytical model to retrieve n from the backscattering ratio and the hyperbolic slope of the particle size distribution, ξ. This latter parameter can be estimated from the spectral dependency of the particle attenuation coefficient (Morel 1973; Boss et al. 2001). While direct measurements of the bulk index of refraction of marine particles are not accessible yet, these studies demonstrated that the retrieved n values from $b_{bp}:b_p$ and ξ are in good agreement with expectation: low n values were found in phytoplankton-dominated waters, whereas high n values were observed in mineral particles–dominated waters, especially in the vicinity of the sediment bed. As far as we know, only Boss et al. (2004) and Chami et al. (2005) tried to evaluate the pertinence of these indirect retrievals of n. They compared the backscattering ratio to the more classical ratio Chl $a:c_p(650)$, a proxy for the relative proportion of phytoplankton within the total particulate mater. Boss et al. (2004) found a significant negative correlation between these two ratios, confirming that a relatively high concentration of phytoplankton (high Chl $a:c_p[650]$) is associated with low bulk refractive index (low $b_{bp}:b_p$). Note, however, that no relationship was observed between $b_{bp}:b_p$ and Chl $a:c_p$ from data collected in the Crimea coastal waters (Chami et al. 2005).

Besides getting information on the marine particle composition and size distribution, the backscattering ratio is also of fundamental importance in marine optics for two other reasons. First, the knowledge of this ratio allows one to derive an approximate scattering phase function of particles (Mobley et al. 2002), which is a key parameter for water radiative transfer computations. Second, this ratio is usually used in many semianalytical algorithms aiming at retrieving the inherent optical properties from radiometric measurements (Gordon et al. 1988; Morel and Maritorena 2001).

In the present study, we analyze the measurements performed during four cruises in the spring and early summer of 2004 in the coastal areas of the eastern English Channel and of the southern North Sea. Our main purpose is to describe and to understand the variability of b_p, b_{bp}, and $b_{bp}:b_p$ during relatively intense phytoplankton bloom episodes in this complex environment characterized by a quasi-permanent background of mineral particles. In particular, we aim at understanding how and to what extent changes in the relative concentrations of particles types affect the $b_{bp}:b_p$ ratio. Whereas a general decreasing of $b_{bp}:b_p$ from mineral- to phytoplankton-dominated waters has already been described, this behavior has never been quantitatively evaluated using simultaneous measurements of biogeochemical variables characterizing the nature of the bulk particulate assemblage. The refractive index values, as calculated from an analytical formulation derived from Mie scattering theory (Twardowski et al. 2001), are also presented and discussed with respect to the composition of the particulate assemblage.

Sampling and methods

Description of the studied area—Four cruises were conducted from March to June 2004 in the inshore and offshore waters of the eastern English Channel and in the inshore waters of the southern North Sea (Fig. 1) as part of

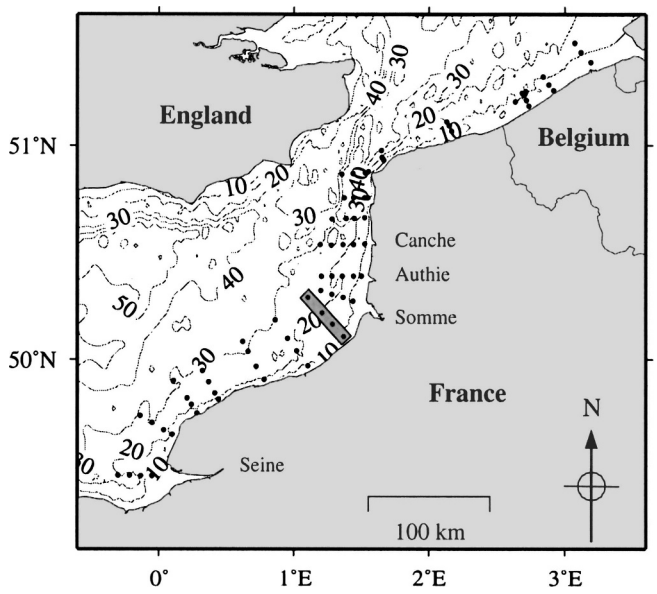

Fig. 1. Location of the stations sampled on 15–18 March, 11–16 April, 10–15 May, and 25–30 June 2004. The 10–50-m isobaths, as well as the main river outlets, are displayed. The gray line southwest of the Somme outlet represents the specific transect described in Fig. 6.

the French National Program of Coastal Environment (PNEC). The location of the sampled stations is indicated in Fig. 1. Each station was not systematically visited during all cruises because of bad weather conditions encountered on some occasions. The English Channel, which is known for its strong hydrodynamics, is usually considered an area of transport of dissolved and particulate matter from the Atlantic to the North Sea. The water circulation in the studied area results from the interactions of a very high tidal regime (tidal range is about 6–9 m in front of the Somme River), intense tidal currents, relatively shallow waters (see isobaths in Fig. 1), and freshwater discharges from different rivers, la Seine and la Somme being the most important ones. All these different geographical and physical characteristics contribute to the establishment of a quasi-permanent background of terrigenous material through either direct inputs (land surfaces and rivers runoff) or resuspension effects. This region is also characterized by relatively intense phytoplankton blooms occurring in spring. Among the different phytoplankton species usually found in this area, the prymnesiophyte *Phaeocystis globosa* is well known for its intrusive behavior along the French and English coasts of the Channel (Bautista et al. 1992; Breton et al. 2000) and in the North Sea (Riegman et al. 1992). This species, presenting a complex life cycle including free-living cell and colony phases, may reveal itself as harmful for the local economy and tourism activities by forming foam aggregates under specific environmental conditions (Lancelot 1995). The cruise periods (15–18 March, 11–15 April, 10–15 May, 25–30 June) were chosen in order to match the *Phaeocystis* bloom initiation, development, and collapse as far as possible. Therefore, because of their important biogeochemical variability, the eastern English Channel waters represent a very interesting environment for the study of the $b_{bp}:b_p$ natural behavior.

CTD and optical measurements—At 229 stations, a conductivity–temperature and depth (CTD) profiler (Sea-Bird) and an optical package (WET Labs) were deployed from surface down to 2–3 m above the bottom. The optical package included a chlorophyll fluorometer, a 10-cm-path-length beam transmissometer (at wavelength $\lambda = 650$ nm), and two ECO-VSF (at $\lambda = 532$ and 650 nm, respectively). All instruments were calibrated by their manufacturer. As this study focused only on the surface layer, full-resolution profiles were averaged over the first 4 m (approximately 20 data points).

The particle attenuation coefficient at 650 nm (m^{-1}) was obtained as follows:

$$c_p(650) = \frac{-\ln(T)}{d} - c_w(650) - a_{ys}(650) \quad (1)$$

where T represents the transmission, d the path length (m), $c_w(650)$ the attenuation coefficient of pure sea water (m^{-1}), and $a_{ys}(650)$ the absorption coefficient of colored dissolved organic matter (m^{-1}) (assuming that scattering by this last is negligible). In order to obtain $a_{ys}(650)$, seawater samples were filtered immediately onboard under low vacuum on a 0.2-μm polycarbonate membrane filter. The absorbance by each filtered sample was then measured in a 10-cm quartz cuvette between 300 and 800 nm with a 1-nm increment using a double-beam spectrophotometer (Uvikon 490; Kontron). Milli-Q water was used as reference water, and the absorbance value over a 5-nm interval around 685 nm was subtracted to each spectrum (Pegau et al. 1997). The absorption by colored dissolved organic matter is then obtained by fitting the following exponential function to the data:

$$a_{ys}(\lambda) = a_{ys}(\lambda_r)\ e^{-S(\lambda - \lambda_r)} \quad (2)$$

where λ_r is a reference wavelength (here $\lambda_r = 443$ nm) and S the spectral slope of $a_{ys}(\lambda)$, which is obtained by a linear regression to the log values of the data in the 350–500 nm spectral range.

At 650 nm, the attenuation by particles is essentially determined by their scattering properties as a_p, the absorption by living and nonliving particles ($c_p = a_p + b_p$), brings only a very small contribution (Loisel and Morel 1998). Because a_p was not measured during our cruises, b_p is directly calculated from c_p using an empirical relationship. Based on previous measurements performed in 2003 during the same period, one may consider that the absorption by particles represents about 4% of $c_p(650)$ in this region and for this particular period (Fig. 2). The particulate scattering coefficient ($b_p[650]$; m^{-1}) is then obtained from $c_p(650)$ as follows:

$$b_p(650) = 0.9755\, c_p(650) - 0.0309 \quad (r^2 = 0.999) \quad (3)$$

The backscattering coefficient by particles, $b_{bp}(650)$ (m^{-1}), is calculated from the ECO-VSF scattering measurements

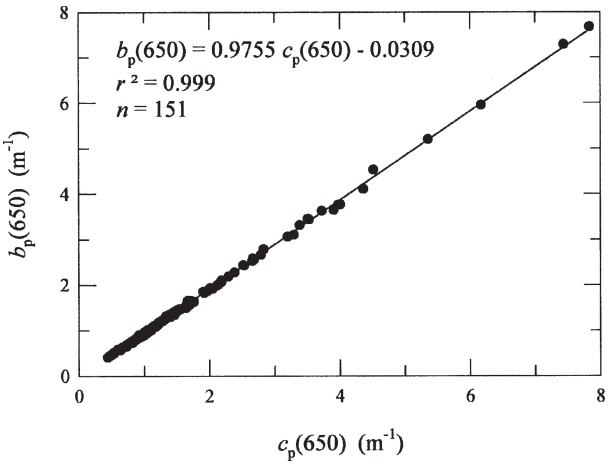

Fig. 2. Scatter plot of particulate scattering $b_p(650)$, measured by the ac-9, as a function of particulate attenuation, $c_p(650)$, measured simultaneously with the transmissometer. This data set was collected during the spring of 2003 in the same area. The solid line is the linear fit for all the data displayed.

performed at 100°, 125°, and 150° as described in Boss et al. (2004). Backscattering by water molecules at each given angle was computed as a function of salinity as in Morel (1974) and subtracted from the measured signal after correction for the loss of photons along the path due to absorption by particulate and dissolved material. Note that this correction does not account for the scattering losses along the path length, as it is already included in the calibration procedure suggested by the manufacturer, which uses a serial concentration of microsphere solutions. Absorption by particulate matter at 650 nm was calculated from Chl *a* using the formulation of Bricaud et al. (1998). This absorption correction was typically less than 1.0% at 650 nm. A third-order polynomial function was then fitted on the three resulting values once multiplied by a $2\pi\sin\theta$ factor (where θ is the scattering angle). Note that this fit also accounts for a fourth point for which the ordinate is zero at $\theta = \pi$ ($2\pi\sin\theta = 0$ for $\theta = \pi$). The backscattering coefficient by particles, b_{bp}, was then derived by integration of this function between 90° and 180°. As only b_p and b_{bp} measured at 650 nm are used here, the wavelength is omitted in what follows, unless specifically indicated.

In June 2004, an ac-9 (WET Labs) and a Hydroscat-6 (HOBI Labs) were also deployed nearly simultaneously with our optical package, allowing the intercomparison of attenuation and backscattering measurements. The ac-9, equipped with a SeaBird 3K pump for water flow into the 25-cm-path-length tubes, performs vertical profile of total (except water) spectral beam attenuation and absorption coefficients $c_{t-w}(\lambda)$ and $a_{t-w}(\lambda)$ (and scattering $b_{t-w} = c_{t-w} - a_{t-w}$) at the nominal wavelengths 412, 440, 488, 510, 532, 555, 650, 676, and 715 nm. On-deck calibrations with Milli-Q water were performed at the beginning and at the end of the campaign (June 2004). The measurements were processed using a homemade software. Temperature and salinity corrections were performed using contemporaneously recorded CTD data (SeaBird SBE 19). The scattering corrections of the measured absorption were performed following method 3 of Zaneveld et al. (1994).

Vertical profiles of the total (including water) backscattering coefficients $b_b(\lambda)$ at the nominal wavelengths 442, 488, 510, 555, 620, and 665 nm were collected with the HydroScat-6. The instrument actually measures the scattering at a single angle in the backward direction (140°), from which, using an empirical relationship, b_b is retrieved (Maffione and Dana 1997). The data conversion from raw to calibrated was performed using the Hydrosoft 2.6 software (HOBI Labs). This conversion relies on calibrations with Milli-Q water performed at JRC-Ispra every 6 months, roughly. In situ attenuation corrections were made using the simultaneously recorded beam attenuation and absorption (ac-9 data). Additionally, binned vertical profiles with 1-m resolution were computed from the full-resolution profiles of *c, b*, and b_b.

Surface water sampling for biogeochemical measurements—On each station, surface water samples were collected just below the surface, using an 8-L Niskin bottle, simultaneously with in situ optical measurements of the backscattering and attenuation coefficients. Filtrations were performed immediately onboard at low vacuum pressure onto 25-mm glass-fiber filters (Whatman GF/F) for subsequent determination of the concentrations of total suspended matter (SPM; g m^{-3}), particulate organic carbon (POC; mg m^{-3}), and chlorophyll *a* (Chl *a*; mg m^{-3}). Each filter was immediately put in a polycarbonate Petri dishes and stored in liquid nitrogen until laboratory analyses. Before filtration for SPM dry-weight and carbon measurements, the filters were precombusted in order to remove any trace of organic matter and then preweighed. Just after filtration, the filters were gently rinsed with Milli-Q water in order to remove residual salt. Note that precombustion shrinks the pore size of the GF/F filters for which it is initially assumed that particles with diameter greater than 0.5–0.7 μm are retained before shrinking. Whereas the JGOFS protocol recommends a 0.4-μm polycarbonate filter for the SPM determination, we decided to use a GF/F filter to be consistent with the POC and Chl *a* measurements. Moreover, the GF/F filters are now commonly employed in many studies involving SPM measurements (Zibordi et al. 2002; Babin et al. 2003). The determination of the SPM dry weight was performed using a Perkin Elmer microbalance. The concentration of particulate organic carbon was determined using a CHN Carbo-Erba elemental analyzer. Note that while SPM includes all organic and mineral material above approximately 0.5–0.7 μm, POC corresponds to autotrophic organisms, heterotrophic bacteria, and detritus. The concentration of Chl *a* was determined by spectrophotometry according to the protocol defined by Lorenzen (1967). Whereas POC : SPM may be used as a rough indicator of the organic fraction of the suspended particulate matter, POC : Chl *a* can be related to the carbon mass of both living and nonliving material with respect to that of autotrophic organisms. Note that POC is converted in g m^{-3} when the ratio to SPM is built.

The index of refraction as derived from $b_{bp}:b_p$—A rough determination of the bulk refractive index, n, can be made according to Twardowski et al. (2001), where n is directly expressed as a function of the backscattering ratio:

$$n = 1 + 1.67\left(b_{bp}/b_p\right)^{0.582} \tag{4}$$

Another, more accurate model was developed by Twardowski et al. (2001) in which both $b_{bp}:b_p$ and the spectral dependency, γ, of the particulate attenuation coefficient, c_p, are used as input parameters:

$$n = 1 + \left(b_{bp}/b_p\right)^{0.5377 + 0.4867(\gamma)^2} \left[1.4676 + 2.2950(\gamma)^2 + 2.3113\,(\gamma)^4\right] \tag{5}$$

These two models present very similar results as far as the slope of the hyperbolic size distribution of particles is between -3.5 and -4 but rapidly diverge out of this range (Twardowski et al. 2001). Concurrent estimations of $b_{bp}:b_p$ and γ derived from in situ measurements of b_{bp}, b_p, and c_p were performed in June 2004 and in the spring of 2003, allowing the direct comparison of the n values computed from the two models. This comparison is performed after subtracting 1 from n and is evaluated in terms of average relative differences, absolute

$$\left(= 100\frac{1}{N}\sum_{1}^{N}\left|\frac{n_{Eq.5} - n_{Eq.4}}{(n_{Eq.5} + n_{Eq.4})/2}\right|\right)$$

or signed

$$\left(= 100\frac{1}{N}\sum_{1}^{N}\frac{n_{Eq.5} - n_{Eq.4}}{(n_{Eq.5} + n_{Eq.4})/2}\right)$$

By considering the whole data set available for this comparison ($N = 156$), the absolute (i.e., uncertainty) and signed (i.e., bias) average relative differences are 22% and -21.6%, respectively. By keeping data points with γ values ranging from -3.5 to -4 ($N = 124$), the agreement is better (uncertainty = 15.2% and bias = -15.4%), as predicted from Mie theory calculations.

Results and discussion

Intercomparison of optical measurements performed with different instruments—A data set including 46 "match-ups" of particulate backscattering, scattering, and backscattering to scattering ratio measurements was constituted from the June 2004 data set. An excellent agreement (slope = 1.045 and $r^2 = 0.976$) is observed between the two sets of b_{bp} data (Fig. 3a), for which the value of the root-mean-square difference in linear scale (RMS) is 0.00223. Particulate backscattering estimated from Hydroscat-6 measurements are on average slightly higher (by 1.54%) than values estimated (after interpolation at 650 nm) from ECO-VSF measurements. The determination coefficient between the two estimates of $b_p(650)$ is slightly lower ($r^2 = 0.868$), $b_p(650)$ measured by the ac-9 being slightly higher

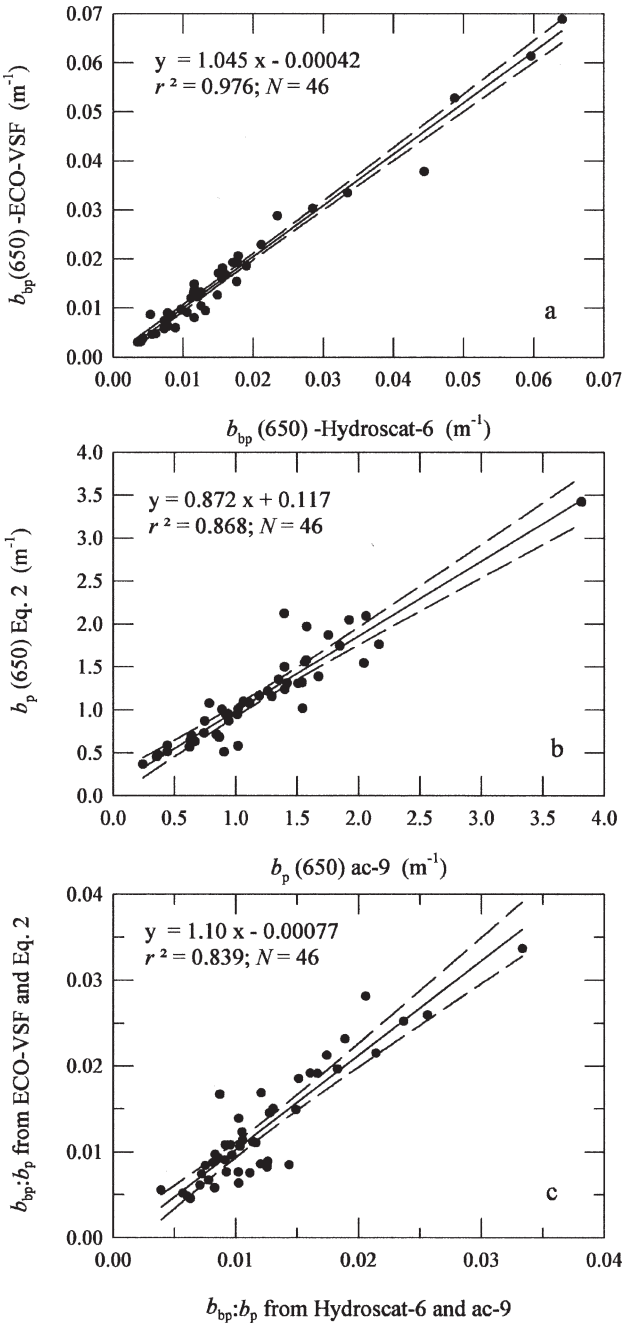

Fig. 3. (a) Comparison of the ECO-VSF and Hydroscat-6 $b_{bp}(650)$ measurements performed in June 2004 within the 0–1.5-m surface layer. Hydroscat-6 values were obtained from the linear interpolation of the measurements performed at 620 and 665 nm. (b) Comparison of the $b_p(650)$ values estimated from the 10-cm-path-length beam transmissometer and from the ac-9 measurements. (c) Comparison of the $b_{bp}:b_p(650)$ ratio values calculated as indicated on each axis. For each panel, the solid line is the linear fit for all the data displayed, and the long dashed lines delimit the 95% confidence interval.

than that estimated from the transmissometer (by 1.49%) (Fig. 3b). The RMS for $b_p(650)$ is 0.228. The results of this comparison remain almost unchanged if the $b_p(650)$ values estimated by the transmissometer are calculated as $c_p(650)$–

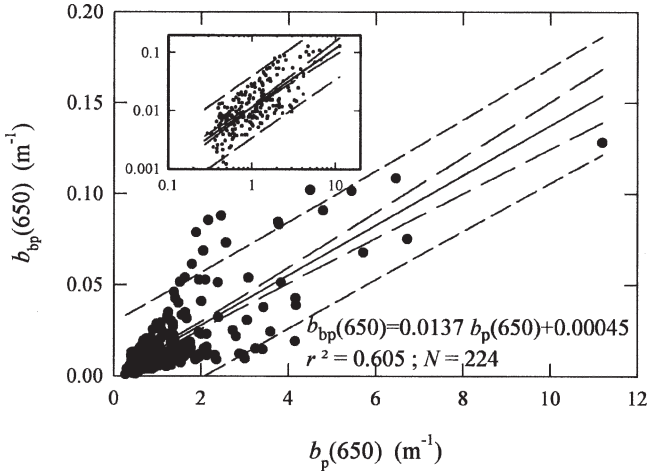

Fig. 4. Scatter plot of $b_{bp}(650)$ versus $b_p(650)$ for the whole data set. The solid black line is the corresponding linear regression, the long dashed lines delimit the 95% confidence interval, and the short dashed lines delimit the prediction interval. The same plot is presented in log-log scale in the inset panel.

$a_p(650)$, where $a_p(650)$ is estimated from Chl *a* (Bricaud et al. 1998) rather than from Eq. 2. The differences in the b_{bp} and b_p measurements compensate one each other when combined into the $b_{bp}:b_p$ ratio for which r^2, RMS, and uncertainty are 0.852%, 0.0028%, and 0.022%, respectively (Fig. 3c). Part of the observed differences in these intercomparisons is attributable to the different designs of the two instruments (e.g., the path-length difference), to the different measurement concepts, and also to the possible time (and consequently space) difference between the two samplings due to strong current drift at some stations.

Natural variability of the relationship between b_{bp} *and* b_p—The linear regression performed on the whole data set ($N = 224$) shows that the relationship ($r^2 = 0.60$) between b_{bp} and b_p at 650 nm is highly scattered (Fig. 4). The mean and standard deviation values of b_{bp} and b_p are 0.0195 ± 0.0233 m^{-1} and 1.39 ± 1.32 m^{-1}, respectively. Note that the coefficient of variation for b_{bp} (1.20) is higher than that of b_p (0.95). The $b_{bp}:b_p$ ratio ranges between 0.0024 and 0.0417, with a mean value of 0.0138 ± 0.0083. This range of variability is consistent with others studies performed in different environments. For example, Twardowski et al. (2001) measured $b_{bp}:b_p$ ranging between 0.002 and 0.03 in the Gulf of California. Similar measurements performed by Boss et al. (2004) in the Mid-Atlantic Bight and by Chang et al. (2004) in the Santa Barbara Channel provided $b_{bp}:b_p$ values spanning over a wide range: 0.005 to 0.035 and 0.002 to 0.075, respectively.

The $b_{bp}:b_p$ ratio is presented in Fig. 5a as a function of Chl *a*, this last being traditionally considered an indicator of the surface water trophic state. As a matter of comparison, previous empirical (Twardowski et al. 2001; Sulivan et al. 2005) and semianalytical (Ulloa et al. 1994; Gordon et al. 1988; Morel and Maritorena 2001) relationships between $b_{bp}:b_p$ and Chl *a* are plotted together with the present individual data. For the semianalytical models b_{bp} and b_p were not measured but computed from surface

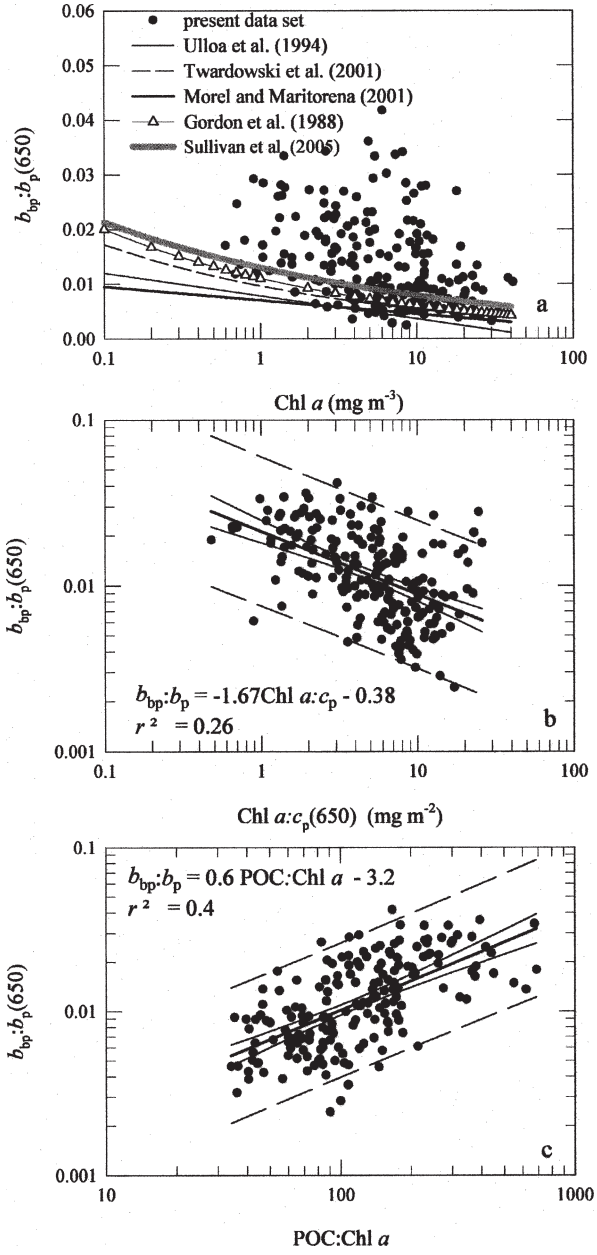

Fig. 5. Plots of (a) the backscattering ratio at 650 nm, $b_{bp}:b_p$, versus the chlorophyll *a* concentration, Chl *a*, for the present data set (filled circles). The four curves represent different published models as indicated. (b) The backscattering ratio at 650 nm versus the ratio of Chl *a* to beam attenuation (at 650 nm), Chl $a:c_p$. (c) The backscattering ratio at 650 nm versus the ratio of the particulate organic carbon to chlorophyll *a*, POC : Chl *a*. In panels (b) and (c), the thick solid line is the linear fit for all the data displayed, the thin solid lines delimit the 95% confidence interval, and the long dashed lines delimit the prediction interval.

reflectance measurements using different assumptions on the respective contributions of living and nonliving suspended particles to the backscattering process. For what concerns the two empirical models, Chl *a* was not measured but estimated from fluorescence in the model of Twardowski et al. (2001) and from the absorption measurements with an ac-9 in the model of Sulivan et al.

(2005). The errors on the chlorophyll values estimated by these two different methods should not exceed ±50%, according to the authors. Despite the strong scatter of our data set, a global decrease of $b_{bp}:b_p$ with increasing Chl *a* is slightly visible ($b_{bp}:b_p = -0.3 \log [\text{Chl } a] - 1.71$; $r^2 = 0.21$), in agreement with previous field studies (Twardowski et al. 2001; Sulivan et al. 2005). Interestingly, the slope, *S* (−0.233), of the hyperbolic fit between $b_{bp}:b_p$ and Chl *a* for our data set is very comparable to those determined by Twardowski et al. (2001) and Sulivan et al. (2005), which are −0.253 and −0.216, respectively. Additionally, our $b_{bp}:b_p$ values are generally greater than those obtained from the other models at any one chlorophyll concentration. This pattern may be explained by a higher concentration of mineral and small particles in our sampled waters, compared to the previous studies.

The backscattering ratio is also presented as a function of the Chl $a:c_p$ ratio (Fig. 5b), which can be considered an indicator of the nature of the bulk particulate matter (Loisel and Morel 1998). Although the relationship is very poor ($r^2 = 0.26$), our results confirm the negative trend found by Boss et al. (2004) between both ratios. Note that $b_{bp}:b_p$ is also found here to be negatively correlated ($r^2 = 0.17$) with the Chl *a*:SPM ratio (not shown). Compared to the evolutions reported in Fig. 4a and Fig. 4b between $b_{bp}:b_p$, Chl *a*, and Chl $a:c_p$, a tighter relationships is found between $b_{bp}:b_p$ and POC:Chl *a* ($r^2 = 0.40$) (Fig. 5c). A positive trend is found between $b_{bp}:b_p$ and the POC:Chl *a* ratio that reveals that the amount of organic material (both living and nonliving, including phytoplankton) relative to autotrophic organisms significantly conditions the backscattering ratio variability. Note that the scatter of data observed in these plots is of the same order than for the previously mentioned relationships. Surprisingly, no relationship was found over the whole data set between $b_{bp}:b_p$ and POC:SPM, a proxy for the respective proportion of organic and inorganic particles (this is not true for individual areas, as shown in Fig. 6). This may be due to (1) uncertainties in the SPM determination (however, the mean value of the scattering coefficient normalized to SPM is 0.9 $m^2\ g^{-1}$, which is consistent with Babin et al. 2003); (2) a narrow range of variability of POC:SPM (20–200) compared with that of Chl *a* and POC:Chl *a*; and (3) the fact that neither Chl *a* nor Chl $a:c_p$, POC:SPM, and POC:Chl *a* may account alone for the whole $b_{bp}:b_p$ variability.

The refractive index calculated from $b_{bp}:b_p$—The mean value of the refractive index (relative to water) resulting from Eq. 4 is equal to 1.133 ± 0.047, which is intermediate between the value expected for a phytoplankton-dominated water and the one for a sediment-dominated water. Indeed, most common mineral present in oceanic waters present a refractive index between 1.14 and 1.26 (Lide 1997), whereas phytoplankton cells present much lower values (1.02–1.092) because of their high water content (Stramski et al. 1988). For the present waters, values higher than 1.2 (the observed maximum value is 1.263) are generally found in front of the river mouths and in very shallow areas. For these stations ($N = 21$), the mean refractive index is 1.218 with a standard deviation of 0.016. The corresponding mean Chl *a*, POC:Chl *a*, and POC:SPM values are 4.8 ± 3.4 mg m^{-3}, 221 ± 149, and 0.057 ± 0.03, respectively. Values lower than 1.10 (the observed minimum value is

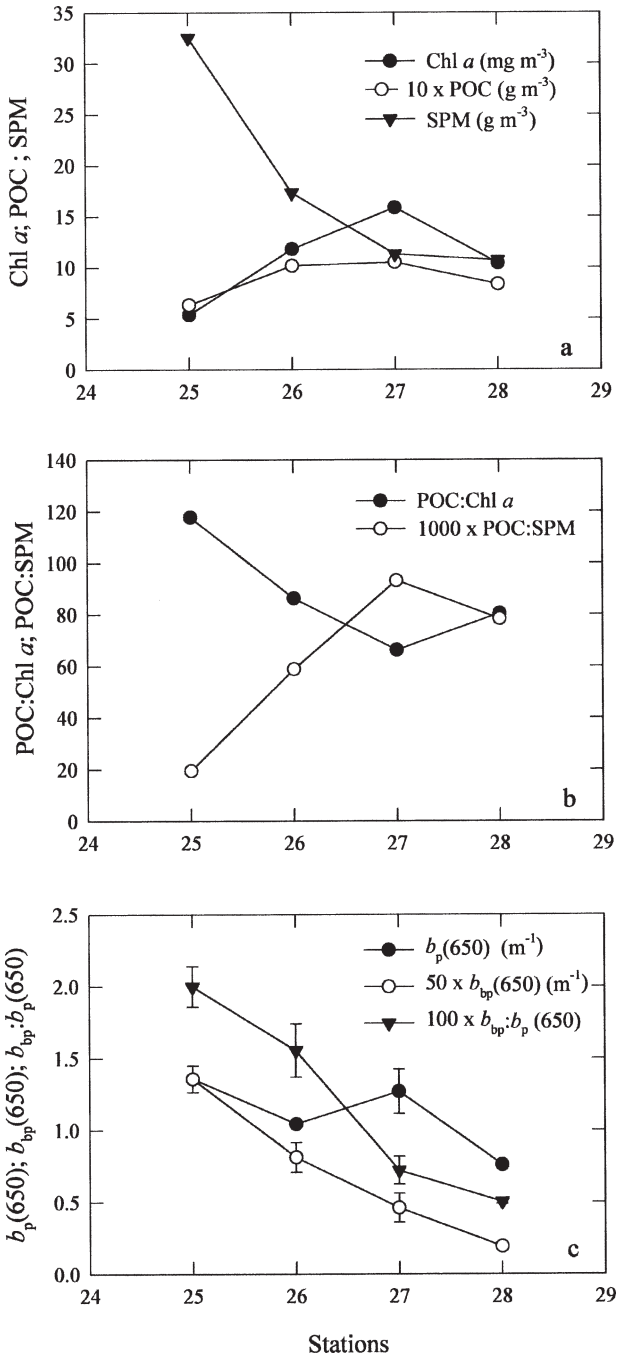

Fig. 6. Surface biogeochemical quantities and optical properties collected along a transect in the bloom area on 12 April 2004 (see Fig. 1). (a) Chl *a*, POC, and SPM as a function of the station number (from nearshore to offshore stations). (b) As panel (a) for POC:SPM and POC:Chl *a*. (c) As panel (a) for the average value of $b_{bp}(650)$, $b_p(650)$, and $b_{bp}:b_p(650)$ in the 0–4-m surface layer. Errors bars in panel (c) represent the scattering and backscattering standard deviations.

1.0504) are essentially found for very high Chl *a* values, and the mean *n* value for these stations is 1.082 ± 0.012 (N = 61). The corresponding Chl *a*, POC : Chl *a*, and POC : SPM mean values are 11.9 ± 7.7 mg m^{-3}, 80 ± 37, and 0.067 ± 0.039, respectively. Therefore, for these two extreme data sets, the agreement between the mean *n* value and the biogeochemical composition of the particulate matter, as roughly defined by Chl *a*, POC : SPM, and POC : Chl *a*, conforms to expectations. However, these two sets present very similar POC : SPM ratio values, indicating that *n* may exhibit a relatively large variability, whereas the proportion between organic and inorganic particles is constant.

Spatial distribution of biogeochemical and optical parameters—The spatial distribution of biogeochemical and optical parameters along a particular transect (the gray line in Fig. 1) performed in the bloom area in April 2004 is examined in Fig. 6 (this transect was chosen, as it is characterized by a great biogeochemical variability). According to microscopic analyses allowing the identification and the quantification of the phytoplankton species, this period corresponds to a transition between a first bloom of diatoms that occurred in March and a second bloom of *P. globosa* that fully developed in May (F. Artigas pers. comm.). Chl *a* and POC increase from coastal (station 25) to offshore (station 28) stations, whereas SPM presents the inverse pattern (Fig. 6a). Chl *a* and SPM vary up to a factor of 3 along the transect, whereas POC varies only by a factor of 1.6. As a consequence, one can observe a strong increase of POC : SPM and, to a lesser extent, a decrease of POC : Chl *a* as the distance from the coast increases (Fig. 6b). Therefore, the organic fraction of the suspended particulate matter increases and is more autotrophic-dominated from nearshore to offshore stations along this specific transect. Regarding the optical parameters, both b_{bp} and b_p reach their lowest values in offshore waters and their highest values in nearshore waters (Fig. 6c), similar to the SPM evolution but opposite of the Chl *a* one. However, note that the b_p evolution is very similar to the Chl *a* one from stations 26 to 28, whereas b_{bp} and SPM have very similar behavior along the whole transect. The relative maximum of b_p observed at station 27 and corresponding to the Chl *a* one is not noticeable for b_{bp}. The excellent agreement between the b_{bp} and SPM spatial trends may be explained by a high proportion of mineral particles in SPM. The $b_{bp} : b_p$ ratio is inversely correlated with the POC : SPM ratio, in excellent agreement with the theory predicting a decrease of $b_{bp} : b_p$ from mineral- to organic-dominated waters. The covariation between $b_{bp} : b_p$ and POC : Chl *a* suggests an increasing proportion of small particles compared to larger ones when the POC : Chl *a* ratio increases as well as a higher refractive index of the detritus and heterotrophic bacteria contributing to POC with respect to living phytoplankton cells. Discussion on these two different aspects related to the nature of the bulk particulate matter will be provided next from the whole data set.

The spatial distributions of Chl *a*, POC : SPM, POC : Chl *a*, b_p, b_{bp}, and $b_{bp} : b_p$ in April 2004 are now compared over the whole investigated region (Fig. 7). The Chl *a* concentration (Fig. 7a) is maximum (~20 mg m^{-3}) over a relatively large area (~1,275 km^2) south of the Somme River as well as along the Belgian coast. The bloom occurring in the eastern English Channel is partly explained by the nutrients input from the Somme River, which presents a maximum outflow in March and April. South of this bloom area, Chl *a* is quite homogeneously distributed and is characterized by relatively low concentrations (average ± standard deviation = 2.8 ± 1.2 mg m^{-3}). In contrast, Chl *a* commonly presents much higher concentration in the northern area, with the highest values (~10 mg m^{-3}) located along the French coasts. The POC : SPM ratio (Fig. 7b) presents a lower variability than Chl *a* as shown by their coefficient of variation equal to 67% and 85%, respectively (Table 1). POC : SPM presents its greatest values along the French coast and in the bloom area (especially on its northern boundary) of the eastern Channel. Note that high Chl *a* values observed within the North Sea are not associated with high POC : SPM values, indicating that resuspended inorganic particles in these very shallow waters (bottom depth between 5 and 10 m) largely contribute to the particulate pool. The POC : Chl *a* and POC : SPM ratios (Fig. 7c) present the same coefficient of variation over the whole studied area (Table 1). Relatively high POC : Chl *a* values (187 ± 91) are generally found south of the Channel bloom area, whereas much lower values are found north of it (95 ± 51).

The particulate scattering and backscattering coefficients present a very similar spatial distribution that clearly differs from that of the chlorophyll concentration (Fig. 7d,e). The b_p and b_{bp} maxima are observed at the southern and northern margins of the studied area, in good correspondence with the SPM maxima located in the outlet of the Seine River (SPM = 40 g m^{-3} at the coastal station and rapidly drops to 4.8 g m^{-3} approximately 9 km offshore) and in the shallow (~5–10-m) Belgian coastal stations (SPM = 44.4 ± 19.4 g m^{-3}), where resuspension of bottom sediment can be important. Note that the b_p and b_{bp} maxima in the North Sea are shifted northern compared to the Chl *a* maximum. The minimum b_p and b_{bp} values are observed offshore and in the central part of the eastern English Channel, in good correspondence with low Chl *a* values. No specific b_p and b_{bp} pattern is associated with the eastern English Channel bloom, especially for b_{bp}. The coefficient of variation of the $b_{bp} : b_p$ ratio is much lower than that of Chl *a* but close to that of POC : Chl *a* and POC : SPM (Table 1). The $b_{bp} : b_p$ spatial distribution in the eastern English Channel is characterized by a north-to-south gradient that is in good agreement with the Chl *a*, POC : SPM, and POC : Chl *a* patterns (Fig. 7f). The greatest $b_{bp} : b_p$ values are found in the extreme north of the whole studied area ($b_{bp} : b_p$ = 0.026 ± 0.003) and in a relatively homogeneous area located south of the Channel bloom ($b_{bp} : b_p$ = 0.024 ± 0.0036) with relatively low Chl *a* (2.97 ± 1.47 mg m^{-3}), low POC : SPM (0.039 ± 0.015) values, and high POC : Chl *a* (169 ± 71) values. Interestingly, the lowest $b_{bp} : b_p$ values (0.0027 ± 0.00026) are located offshore the Authie River, where the Chl *a* content (7.74 ± 1.15 mg m^{-3}) is almost three times lower than the maximum values found in the bloom area. This indicates

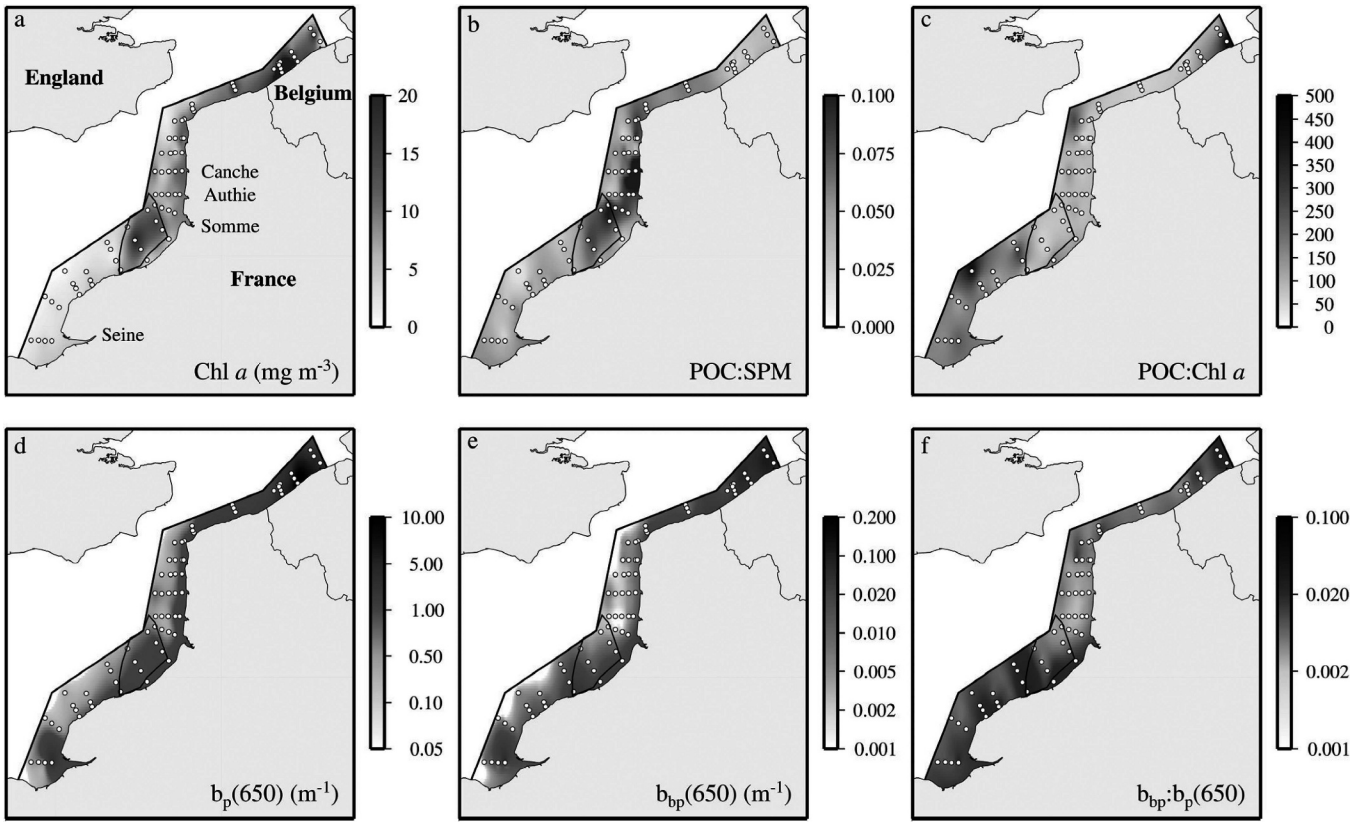

Fig. 7. Spatial distribution of (a) Chl *a*, (b) POC : SPM, (c) POC : Chl *a*, (d) $b_p(650)$, (e) $b_{bp}(650)$, and (f) $b_{bp} : b_p(650)$ in April 2004. The contour line on each panel delimits the bloom area. The white dots represent the stations visited in April 2004.

that the usual assumption of a general decreasing of $b_{bp} : b_p$ with increasing Chl *a* is not always fully confirmed. The POC : SPM (0.067 ± 0.031) and the relatively small POC : Chl *a* (94.8 ± 7) values may contribute to explain part of this pattern.

The seasonal variability within the b_{bp}–b_p relationships—The b_{bp}–b_p relationship is now specifically examined in correspondence with the variability of Chl *a*, POC : SPM and POC : Chl *a*. For that purpose, b_{bp} is plotted as a function of b_p for each cruise (Fig. 8). In March, one can observe a quasi-linear relationship between b_{bp} and b_p (r^2 = 0.88), with a relatively weak scatter around the general trend line (Fig. 8a). The mean $b_{bp} : b_p$ value (0.0199 ± 0.0078) is very close to the mean value (~0.018) derived from the Petzold's measurements performed in 1973 in San Diego Harbor and extensively used in oceanic radiative transfer studies.

From March to April, the mean $b_{bp} : b_p$ value drops by a factor of 1.55 to reach a mean value of 0.0128 ± 0.0079. This decreasing rate is remarkably similar to the Chl *a* increasing rate (~1.54), which suggests that Chl *a* may be the main factor influencing the $b_{bp} : b_p$ temporal variability from March to April. Interestingly, the POC : SPM ratio remains constant over the same period, indicating that the proportion between organic and mineral particles does not change despite the increasing phytoplankton biomass (Table 1). The increasing mineral fraction between March and April may result from the combination of increasing river outflow (bringing new nutrients) and important bottom resuspension due to some strong wind episodes in April. In contrast to the POC : SPM ratio, the POC : Chl *a* ratio decreases by a factor of 1.26, indicating that autotrophic particles represent an increasing fraction of the particulate organic matter in the investigated area. In April, the linear relationship between b_{bp} and b_p is degraded (r^2 =

Table 1. Mean and standard deviation values of Chl *a*, POC : SPM, POC : Chl *a*, and $b_{bp} : b_p$ calculated over the whole studied area and for each cruise. The coefficient of variation (standard deviation divided by the mean times 100%) is given for each case in parentheses.

	Chl *a*	POC : SPM	POC : Chl *a*	$b_{bp} : b_p$
March	5.54±4.3 (77.6%)	0.055±0.033 (60%)	159±168 (105%)	0.0199±0.0078 (39%)
April	8.53±7.25 (85%)	0.055±0.037 (67%)	126±87 (69%)	0.0128±0.0079 (62%)
May	11.3±8.4 (74%)	0.063±0.064 (101%)	125±101 (81%)	0.0110±0.0071 (64%)
June	6.18±5.54 (90%)	0.079±0.031 (39%)	157±106 (67%)	0.0145±0.0084 (58%)

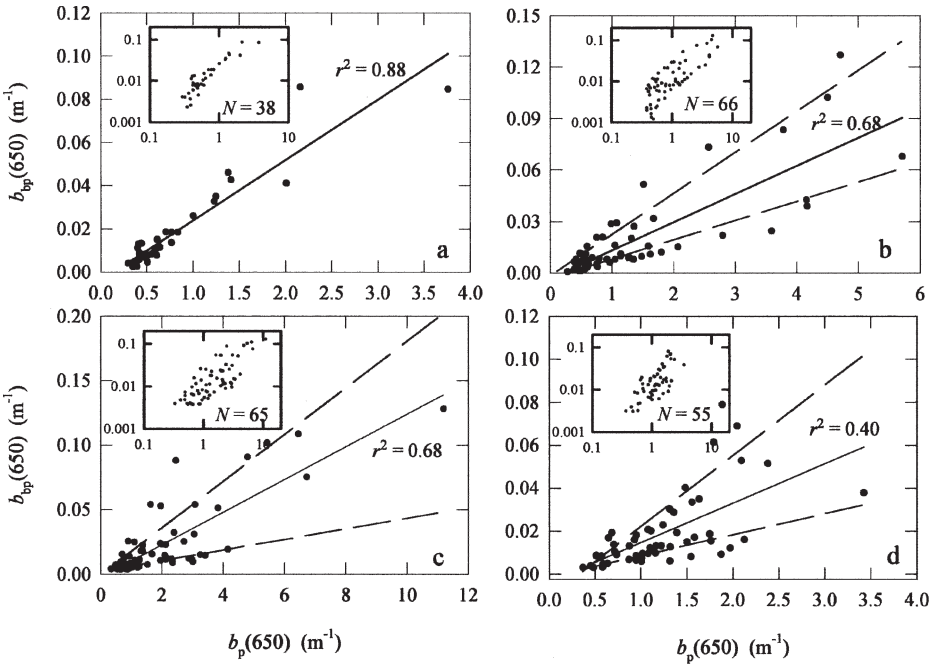

Fig. 8. Scatter plot of $b_{bp}(650)$ as a function of $b_p(650)$ in (a) March, (b) April, (c) May, and (d) June 2004. *n* represents the number of station visited during each cruise and for which all parameters are available. Note that by conserving the same stations in the two data sets, we checked that the temporal variability observed between March and April is only weakly affected by the number of sampling stations that differs between these two cruises. The solid line drawn on each panel represents the best linear fit over the whole data set collected during the given period, whereas the dashed lines represent the best linear fits for each of two groups. These two groups correspond to the upper and lower data sets segregated with respect to the global regression.

0.68), and the data points are considerably scattered around the general trend line as illustrated by the coefficient of variation of $b_{bp}:b_p$, which increases by a factor of 1.6 (Fig. 8b; Table 1) from March to April. However, these data points appear distributed in two groups characterized by very different mean $b_{bp}:b_p$ values (Table 2). These two groups present significantly different mean $b_{bp}:b_p$ values equal to 0.0076 ± 0.0029 and 0.0214 ± 0.0054, respectively ($r^2 = 0.95$ for regressions performed on both subsets). They also remarkably differ with respect to their biogeochemical parameters (Table 2). Indeed, between the first and the second group, the mean values of $b_{bp}:b_p$, Chl *a*, POC : SPM, and POC : Chl *a* vary by a factor of 2.8, 0.6, 0.53, and 2.1, respectively. This is consistent with expectations, as the group that gathered the lowest $b_{bp}:b_p$ values is characterized by the highest mean Chl *a* and POC : SPM values and the lowest mean POC : Chl *a* value (and vice versa). Note that the two groups seem to correspond to two different water masses as expressed by the salinity: the lowest $b_{bp}:b_p$ values are found in the saltiest waters (Table 2). This pattern may correspond to the presence of the "coastal flow" along the French coast, characterized by low-salinity waters due to continental runoffs and often well delimited seaward by a moving frontal zone (Brylinski et al. 1996).

From April to May, the $b_{bp}:b_p$ ratio keeps decreasing (but only by a factor of 1.16), and the chlorophyll concentration increases by a factor of 1.32, as an intense bloom of *P. globosa* covers a relatively large area northern of the Somme outlet. The POC : SPM ratio increases by

Table 2. Mean and standard deviation values of S, T, Chl *a*, POC : SPM, POC : Chl *a*, and $b_{bp}:b_p$ for the two groups of data points as appearing in Fig. 8 for the April, May, and June cruises. The first (second) group, as referred to in text, is characterized by the lowest (highest) mean $b_{bp}:b_p$ values and corresponds to the first (second) line of each time period. The *N* value corresponds to the number of data points of each group.

	N	S	T (°C)	Chl *a*	POC : SPM	POC : Chl *a*	$b_{bp}:b_p$
April	40	34.15±0.92	9.2±0.3	10.04±7.35	0.069±0.042	88±37	0.0076±0.0029
	26	33.28±1.32	9.1±0.3	5.71±5.04	0.036±0.016	189±108	0.0214±0.0054
May	32	34.20±0.66	11.1±0.2	14.7±8.4	0.051±0.026	64±26	0.006±0.0018
	30	33.53±1.83	11.3±0.5	6.1±5.1	0.074±0.089	200±118	0.017±0.007
June	31	34.05±0.97	16.1±0.6	7.53±7.62	0.080±0.032	123±46	0.0085±0.002
	24	34.07±0.70	16.3±0.8	4.81±2.48	0.076±0.028	204±137	0.022±0.007

a factor of 1.15 from April to May, whereas the POC : Chl *a* ratio is constant (Table 1). This indicates that, on average, the concentration of particulate carbon increases in parallel with the phytoplankton biomass between these two cruises. Two groups are also observed with respect to the b_{bp}–b_p relationship in May (Fig. 8c). The mean values of $b_{bp}:b_p$, Chl *a*, POC : SPM, and POC : Chl *a* vary by a factor of 2.8, 0.4, 1.45, and 3.1 between the first and the second group, respectively (Table 2). The variation of the mean $b_{bp}:b_p$ values between the two groups is similar in April and in May (a factor of 3), which is not the case for the biogeochemical parameters, especially the POC : SPM ratio. The unexpected association of the greatest $b_{bp}:b_p$ values with the greatest POC : SPM values observed in May (and vice versa) suggests that the proportion between mineral and organic matter does not always control the $b_{bp}:b_p$ behavior. In this particular case, the POC : Chl *a* ratio seems to be the main factor (with Chl *a*) to explain the $b_{bp}:b_p$ variability between the two groups observed in May. In contrast to the situation encountered in April, the two groups are more spatially ordered. The stations belonging to the group with the lowest mean $b_{bp}:b_p$ value are generally found in the bloom area of the eastern English Channel, whereas stations in the North Sea all belong to the second group.

From May to June, the mean $b_{bp}:b_p$ value increases up to a value that ranges between those of March and April (Table 1). This is in good correspondence with the Chl *a* and POC : Chl *a* temporal patterns but not with that of POC : SPM. Similarly to the April and May data set, the scatter of the June data points may also be distributed in two groups (Fig. 8d). The mean values of $b_{bp}:b_p$, Chl *a*, POC : SPM, and POC : Chl *a* vary by a factor of 2.6, 0.64, 0.95, and 1.66 between the first and the second group, respectively (Table 2). Therefore, rather than the proportion between organic and mineral particles, which is constant between the two groups, it seems that the nature of the organic particulate matter, as seen through the POC : Chl *a* ratio, as well as the chlorophyll concentration, has the greatest impact on the $b_{bp}:b_p$ variability. In contrast to what we observed in April and May, the two groups present very similar salinity mean value. This may be related to the diminution of river outflows, which is also confirmed by the decrease of SPM from May to June.

In general, the temporal variability of the chlorophyll concentration averaged over the whole study area drives the variability of the backscattering ratio from March to June; that is, Chl *a* increases when $b_{bp}:b_p$ decreases (Table 1). In contrast, the seasonal variations of POC : Chl *a* and POC : SPM have a smaller impact on the $b_{bp}:b_p$ seasonal course. This is mostly due to the much lower temporal variability of POC : Chl *a* and POC : SPM compared with that of Chl *a* during the sampling period. For a given cruise, the large scatter observed in the b_{bp}–b_p relationship is relatively well explained by the variable biogeochemical composition of the bulk particulate assemblage. The highest (lowest) mean $b_{bp}:b_p$ values are always encountered in waters with the lowest (highest) chlorophyll content and the highest (lowest) POC : Chl *a* values. The scatter in the b_{bp}–b_p relationship may also be explained by the proportion of organic and mineral particles, but only when this proportion is significantly variable, such as the situation during April.

The different behaviors reported between the particulate backscattering ratio and the biogeochemical measurements reflect the variability of the bulk particulate matter in terms of size distribution and chemical composition (i.e., refractive index). The increase of $b_{bp}:b_p$ as POC : Chl *a* increases would suggest a higher refractive index of detritus cells compared to phytoplankton cells and an increasing proportion of small particles relatively to large particles in water. Nonliving organic detrital material (NODM) would indeed be characterized by high refractive index (1.15–1.20) in absence of interstitial water. However, even if the particle has little water content when initially generated, water will rapidly penetrate into the particle via osmosis (as long as the particle is permeable) until there is a balance of osmotic pressure and the adhesive forces keeping the particle together. This conforms with the microscopy observations of Verity et al. (1996) as well as to previous estimations of the NODM refractive index that showed that NODM and living organic material (phytoplankton and heterotrophic bacteria) have similar refractive index (Morel and Ahn 1990; Bricaud et al. 1995; Twardowski et al. 2001). Therefore, the refractive index variability may not be the main factor explaining the parallel change of $b_{bp}:b_p$ and POC : Chl *a* in the studied area. However, the NODM particles could also act as scavengers (through adsorption) of minerals particles, these last enhancing the bulk refractive index and consequently the $b_{bp}:b_p$ ratio.

In the absence of bloom episodes, it is usually assumed that the particle size distribution (PSD) of living and nonliving suspended particles can be approximated by a power law or a Junge-type distribution (Jonasz 1983). During phytoplankton blooms, the PSD flattens because of the abundance of typically large (>10 μm) phytoplankton cells, and colonies. Therefore, changes in the phytoplankton community affect the PSD slope and then the $b_{bp}:b_p$ ratio, accordingly. For example, given a particle population characterized by a bulk refractive index of 1.10, the $b_{bp}:b_p$ ratio is expected to decrease by 50% when the PSD slope decreases from 4 to 3 (Fig. 9). The covariation between $b_{bp}:b_p$ and POC : Chl *a* would then suggest that the proportion of relatively small particles increases as POC : Chl *a* increases. This is consistent with the prediction of an increase of the PSD slope when POC is originating predominantly from NODM. The PSD variability can also explain some of the unexpected patterns observed between $b_{bp}:b_p$ and POC : SPM. The observed difference of $b_{bp}:b_p$ between the two groups of data collected in June (Fig. 8d) while POC : SPM remains stable (suggesting a constant refractive index for the two groups) could also be due to a change in PSD.

The availability of the ac-9 and ECO-VSF sensors during the last cruise (25–30 June) allows us to derive an estimate of the PSD slope (ξ) simultaneously with the $b_{bp}:b_p$ ratio. Many studies have indeed shown that the spectral dependency (γ) of the particulate attenuation coefficient, $c_p(\lambda)$, is closely related to ξ (see references in

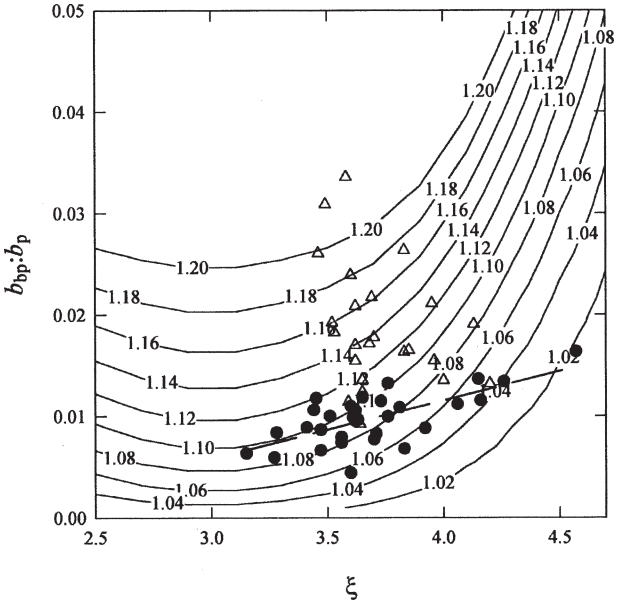

Fig. 9. Particulate backscattering ratio ($b_{bp}:b_p$) versus PSD slope (ξ) from data collected during the last cruise (25–30 June) when both the ac-9 and the ECO-VSF instruments were available. The open triangles and black dots represent the sets of data with the highest and lowest mean POC : Chl *a* values, respectively (see text). The solid curves overlaid on this plot represent the refractive index contours as calculated by the model of Twardowski et al. (2001), which uses $b_{bp}:b_p$ and ξ as input parameters. The long dashed black line corresponds to the best linear fit to the data points represented by black dots.

Twardowski et al. 2001). Based on Mie scattering calculations, different empirical relationships between γ and ξ were then built (Morel 1973; Boss et al. 2001). Here, we use the model of Boss et al. (2001) to convert the γ values derived from the ac-9 measurements into ξ. The $b_{bp}:b_p$ ratio measured during this cruise are plotted against ξ, with the bulk refractive index values calculated from the model of Twardowski et al. (2001) as a background (Fig. 9). Remarkably, the two groups identified in Fig. 8d present a different behavior with respect to n and ξ. For the first group, characterized by the lowest mean POC : Chl *a* value (Table 2), the backscattering ratio variability is driven mainly by ξ ($b_{bp}:b_p = 0.0057\ \xi - 0.011$, $r^2 = 0.46$), whereas n falls within a narrow range of variability (1.02–1.12). In contrast, the stations belonging to the second group are characterized by a relatively small range of variability in ξ (3.5–4.2) but fall within a much higher range of values for n (1.04–1.22). Therefore, whereas the PSD slope is the main factor controlling the $b_{bp}:b_p$ variability in waters where POC is originating mainly from autotrophic organisms (i.e., low POC : Chl *a* values), it appears that n governs $b_{bp}:b_p$ in waters where POC comes from NODM and heterotrophic organisms (i.e., high POC : Chl *a* values). Assuming that NODM and phytoplankton have similar refractive index, this pattern could be explained by aggregation of mineral and nonliving organic detrital material. Additional data are however needed to confirm this assumption observed in our studied area during a postbloom period.

In this paper, we show that the backscattering ratio, $b_{bp}:b_p$, exhibits relatively large variability within the eastern English Channel and southern North Sea. The range of variability reported here is in good agreement with previous studies performed in different coastal and oceanic environments (Twardowski et al. 2001; Boss et al. 2004; Chang et al. 2004). Values as low as 0.003 are found during intense phytoplankton blooms period, whereas values as high as 0.04 are found in front of river mouths or in very shallow waters where resuspension of sediments is important. This is consistent with current knowledge suggesting that low $b_{bp}:b_p$ values are expected for a particle population dominated by low refractive index material such as phytoplankton, whereas high $b_{bp}:b_p$ values are generally observed in presence of a relatively high concentration of inorganic particles. Besides information on bulk particle composition, the large $b_{bp}:b_p$ dynamic range reflects the variability of the particle phase function and then strongly emphasizes that the use of a unique phase function is not appropriated for radiative transfer studies in the coastal environment (even in limited space and time studies). The general decreasing of $b_{bp}:b_p$ with Chl *a* is roughly confirmed (Fig. 6a; Tables 1, 2). However, the data are considerably scattered around the general trend line. As expected, the proportion between organic and mineral matter (i.e., the POC : SPM ratio) partly explains this pattern (Figs. 6, 8b). However, this is not always the case, as illustrated by situations such as those encountered in June (Fig. 8d). Moreover, by pooling all the data together, no significant relationships appear between $b_{bp}:b_p$ and POC : SPM. In contrast, the POC : Chl *a*, which is a rough descriptor of the amount of organic material (both living and nonliving, including phytoplankton) relative to autotrophic organisms, seems to have a great impact on the $b_{bp}:b_p$ behavior in the investigated area: a relatively greater proportion of detritus (and heterotrophic bacteria) compared with that of autotrophic organisms enhances $b_{bp}:b_p$ value (and vice versa). The pattern may be explained by changes in the size distribution of living and nonliving particles as well as by aggregation of mineral and nonliving organic detrital material. However, other factors may also contribute to explain the reported $b_{bp}:b_p$ variability. Among others, one may cite (1) the small particles that are not collected on the filters but that contribute to the measured backscattering and scattering coefficients and (2) the different sizes, structures (i.e., in-heterogeneity), and shapes of organic and mineral particles. For example, the scattering cross section of phytoplankton cells is greater for spherical than for nonspherical cells, whereas the reverse pattern is observed for the backscattering cross-section (Kim and Philpot 2001), which suggests that $b_{bp}:b_p$ is greater for nonspherical than for spherical cells. Similarly to the effect of the organic coatings on the bubble surface that are known to increase $b_{bp}:b_p$ (Zhang et al. 2002), the presence of mucilage associated with the development of the bloom of *P. globosa* also has certainly a great effect on $b_{bp}:b_p$. Note that the impact of a mucilage event on marine optical measurements has already been observed in the Adriatic Sea (Berthon and Zibordi 2000). Researches are underway to evaluate the sensitivity of the backscattering

ratio measured in situ, during the bloom periods, with regard to the nature of the phytoplankton structure (nature, size, and shape of the dominant species).

References

Babin, M., A. Morel, V. Fournier-Sicre, F. Fell, and D. Stramski. 2003. Light scattering properties of marine particles in coastal and open ocean waters as related to the particle mass concentration. Limnol. Oceanogr. **48:** 843–859.

Barnard, A. H., W. S. Pegau, and J. R. V. Zaneveld. 1998. Global relationships of the inherent optical properties of the oceans. J. Geophys. Res. **103:** 24955–24968.

Bautista, B., R. P. Harris, P. R. G. Tranter, and D. Harbour. 1992. *In situ* copepod feeding and grazing rates during a spring bloom dominated by *Phaeocystis* sp. in the English Channel. J. Plankton Res. **14:** 691–703.

Berthon, J.-F., G. Zibordi, and S. B. Hooker. 2000. Marine optical measurements of a mucilage event in the northern Adriatic Sea. Limnol. Oceanogr. **45:** 322–327.

Boss, E., W. S. Pegau, M. Lee, M. Twardowski, E. Shybanov, G. Korotaev, and F. Baratange. 2004. Particulate backscattering ratio at LEO 15 and its use to study particle composition and distribution. J. Geophys. Res. **109.** [doi: 10.1029/2002JC001514]

———, M. S. Twardowski, and S. Herring. 2001. Shape of the particulate beam attenuation spectrum and its inversion to obtain the shape of the particulate size distribution. Appl. Opt. **40:** 4885–4893.

Breton, E., C. Brunet, B. Sautour, and J.-M. Brylinski. 2000. Annual variations of phytoplankton biomass in the Eastern English Channel: Comparison by pigment signatures and microscopic counts. J. Plankton Res. **22:** 1423–1440.

Bricaud, A., A. Morel, M. Babin, K. Allali, and H. Claustre. 1998. Variations of light absorption by suspended particles with the chlorophyll *a* concentration in oceanic (case 1) waters: Analysis and implications for bio-optical models. J. Geophys. Res. **103:** 31033–31044.

———, C. Roesler, and J. R. V. Zaneveld. 1995. In situ methods for measuring the inherent optical properties of ocean waters. Limnol. Oceanogr. **40:** 393–410.

Brown, O. B., and H. R. Gordon. 1973. Comment on "Method For Determination of the Index of Refraction of Particles Suspended in the Ocean." J. Opt. Soc. Am. **63:** 1616–1617.

Brylinski, J-M., C. Brunet, D. Bentley, G. Thoumelin, and D. Hilde. 1996. Hydrography and phytoplankton biomass in the eastern English Channel in spring 1992. Estuar. Coast. Shelf Sci. **43:** 507–519.

Chami, M., and others. 2005. Optical properties of the particles in the Crimea coastal waters (Black Sea). J Geophys Res **110:** C11020. [doi:10.1029/2005JC003008]

Chang, G. C., A. Barnard, R. Zaneveld, C. Moore, T. Dickey, P. Egli, and A. Hanson. 2004. Bio-optical relationships in the Santa Barbara Channel: Implications for remote sensing, p. 1–12. *In* Proceedings of the Ocean Optics XVII Conference. Fremental, Australia.

Claustre, H., A. Morel, M. Babin, C. Cailliau, D. Marie, J.-C. Marty, and D. Vaulot. 1999. Variability in particle attenuation and stimulated fluorescence in the tropical and equatorial Pacific: Scales, patterns and some biogeochemical implications. J. Geophys. Res. **104:** 3401–3422.

Gardner, W. D., I. D. Walsh, and M. J. Richardson. 1993. Biophysical forcing of particle production and distribution during a spring bloom in the North Atlantic. Deep-Sea Res II **42:** 757–775.

Gordon, H. R., O. B. Brown, R. E. Evans, J. W. Brown, R. C. Smith, K. S. Baker, and D. K. Clark. 1988. A semi-analytic radiance model of ocean color. J. Geophys. Res. **93:** 10909–10924.

Gould, R. W., R. A. Arnone, and P. M. Martinolich. 1999. Spectral dependence of the scattering coefficient in case 1 and case 2 waters. Appl. Opt. **38:** 2377–2383.

Jonasz, M. 1983. Particles size distributions in the Baltic. Tellus **35:** 346–358.

Kim, M., and W. D. Philpot. 2001. Optical modeling of phytoplankton: Comparison between spherical and nonspherical models, p. 345–349. *In* I. Levin and G. Gilbert [eds.], Current problems in optics of natural waters. Academic.

Kitchen, J. C., and J. R. Zaneveld. 1990. On the non-correlation of the vertical structure of light scattering and chlorophyll *a* in case I waters. J. Geophys. Res. **95:** 20237–20246.

———, and ———. 1992. A three-layered sphere model of the optical properties of phytoplankton. Limnol. Oceanogr. **37:** 1680–1690.

Lancelot, C. 1995. The mucilage phenomenon in the continental coastal waters of the North Sea. Sci. Total Environ. **165:** 83–102.

Lide, D. R. 1997. Physical and optical properties of minerals, p. 4130–4136. *In* CRC Press [ed.], CRC handbook of chemistry and physics, 77th ed. CRC Press.

Loisel, H., and A. Morel. 1998. Light scattering and chlorophyll concentration in case 1 waters: A reexamination. Limnol. Oceanogr. **43:** 847–858.

Lorenzen, C. J. 1967. Determination of chlorophyll and pheopigments: Spectrophotometric equations. Limnol. Oceanogr. **12:** 343–346.

Maffione, R. A., and D. R. Dana. 1997. Instruments and methods for measuring the backward-scattering coefficient of ocean waters. Appl. Opt. **36:** 6057–6067.

McLeroy-Etheridge, S. L., and C. S. Roesler. 1998. Are the inherent optical properties of phytoplankton responsible for the distinct ocean colors observed during harmful algal blooms? Ocean Opt. **14:** 109–116.

Mobley, C. D., K. S. Lydia, and E. Boss. 2002. Phase function effects on oceanic light fields. Appl. Opt. **41:** 1035–1049.

Morel, A. 1973. Diffusion de la lumière par les eaux de mer. Résultats expérimentaux et approche théorique, p. 3.1-1–3.1-76. *In* Optics of the sea. AGARD Lectures Series.

———. 1974. Optical properties of pure water and pure seawater, p. 1–24. *In* N. G. Jerlov and E. Steeman Nielsen [eds.], Optical aspects of oceanography. Academic.

———, and Y.-H. Ahn. 1990. Optical efficiency factors of free-living bacteria: Influence of bacterioplankton upon the optical properties and particulate carbon in oceanic waters. J. Mar. Res. **48:** 145–175.

———, and Y-H. Ahn. 1991. Optics of heterotrophic nanoflagellates and ciliates: A tentative assessment of their scattering role in oceanic waters compared to those of bacterial and algal cells. J. Mar. Res. **49:** 177–202.

———, and S. Maritorena. 2001. Bio-optical properties of oceanic waters: A reappraisal. J. Geophys. Res. **106:** 7763–7780.

Pegau, W. S., G. Deric, and J. R. V. Zaneveld. 1997. Absorption and attenuation of visible and near-infrared light in water: Dependence on temperature and salinity. Appl. Opt. **36:** 6035–6046.

Riegman, R., A. M. Noordeloos, and G. C. Cadee. 1992. *Phaeocystis* blooms and eutrophication of the continental coastal zones of the North Sea. Mar. Biol. **112:** 479–484.

Stramski, D., E. Boss, D. Bogucki, and K. J. Voss. 2004. The role of seawater constituents in light backscattering in the ocean. Prog. Oceanogr. **61:** 27–56.

———, and D. A. Kiefer. 1991. Light scattering by microorganisms in the open ocean. Prog. Oceanogr. **28:** 343–383.

———, A. Morel, and A. Bricaud. 1988. Modeling the light attenuation and scattering by spherical phytoplanktonic cells: A retrieval of the bulk refractive index. Appl. Opt. **27:** 3954–3956.

Sullivan, J. M., M. S. Twardowski, P. L. Donaghay, and S. A. Freeman. 2005. Use of optical scattering to discriminate particle types in coastal waters. Appl. Opt. **44:** 1667–1680.

Twardowski, M. S., E. Boss, J. B. Macdonald, W. S. Pegau, A. H. Barnard, and J. R. V. Zaneveld. 2001. A model for estimating bulk refractive index from optical backscattering ratio and the implications for understanding particle composition in case I and case II waters. J. Geophys. Res. **106:** 14129–14142.

Ulloa, O., S. Sathyendranath, and T. Platt. 1994. Effect of the particle-size distribution on the backscattering ratio in seawater. Appl. Opt. **30:** 7070–7077.

Vaillancourt, R. D., C. W. Brown, R. R. L. Guillard, and W. M. Balch. 2004. Light backscattering properties of marine phytoplankton: Relationships to cell size, chemical composition and taxonomy. J. Plankton Res. **26:** 191–212.

Verity, P. G., T. M. Beatty, and S. C. Williams. 1996. Visualization and quantification of plankton and detritus using digital confocal microscopy. Aquat. Microb. Ecol. **10:** 55–67.

Zaneveld, J. R. V., and J. C. Kitchen. 1995. The variation in the inherent optical properties of phytoplankton near an absorption peak as determined by various models of cell structure. J. Geophys. Res. **100:** 13309–13320.

———, ———, and C. Moore. 1994. The scattering error coefficient of reflective absorption measurements, p. 44–54. *In* Proceedings of the Ocean Optics XII Conference, SPIE-2258.

Zhang, X., M. Lewis, M. Lee, B. Johnson, and G. Korotaev. 2002. The volume scattering function of natural bubble populations. Limnol. Oceanogr. **47:** 1273–1282.

Zibordi, G., J.-F. Berthon, J. P. Doyle, S. Grossi, D. van den Linde, C. Targa, and L. Alberotanza. 2002. Coastal atmosphere and sea time-series (CoASTS), part 1: A tower-based, long-term measurement program. SeaWiFS Post-launch Technical Report Series **19:** 1–29.

Received: 14 December 2005
Accepted: 28 July 2006
Amended: 13 October 2006